



**HAL**  
open science

## Silicon Nanowire Solar Cells with $\mu\text{c-Si:H}$ Absorbers for Radial Junction Devices

Letian Dai, Martin Foldyna, J Alvarez, Isabelle Maurin, Jean-Paul Kleider,  
Thierry Gacoin, Pere Roca ICabarrocas

► **To cite this version:**

Letian Dai, Martin Foldyna, J Alvarez, Isabelle Maurin, Jean-Paul Kleider, et al.. Silicon Nanowire Solar Cells with  $\mu\text{c-Si:H}$  Absorbers for Radial Junction Devices. *Physica Status Solidi A (applications and materials science)*, 2021, 218 (17), pp.2100231. 10.1002/pssa.202100231 . hal-03289620

**HAL Id: hal-03289620**

**<https://hal.science/hal-03289620v1>**

Submitted on 3 Nov 2021

**HAL** is a multi-disciplinary open access archive for the deposit and dissemination of scientific research documents, whether they are published or not. The documents may come from teaching and research institutions in France or abroad, or from public or private research centers.

L'archive ouverte pluridisciplinaire **HAL**, est destinée au dépôt et à la diffusion de documents scientifiques de niveau recherche, publiés ou non, émanant des établissements d'enseignement et de recherche français ou étrangers, des laboratoires publics ou privés.

# Silicon nanowire solar cells with $\mu\text{-Si:H}$ absorbers for radial junction devices

Letian Dai<sup>a,b,c,d</sup>, Martin Foldyna<sup>c</sup>, José Alvarez<sup>a,b</sup>, Isabelle Maurin<sup>d</sup>, Jean-Paul Kleider<sup>a,b</sup>, Thierry Gacoin<sup>d</sup> and Pere Roca i Cabarrocas<sup>c</sup>

<sup>a</sup>Université Paris-Saclay, CentraleSupélec, CNRS, Laboratoire de Génie Electrique et Electronique de Paris, 91192, Gif-sur-Yvette, France

<sup>b</sup>Sorbonne Université, CNRS, Laboratoire de Génie Electrique et Electronique de Paris, 75252, Paris, France

<sup>c</sup>LPICM, CNRS, Ecole Polytechnique, Institut Polytechnique de Paris, 91128 Palaiseau, France

<sup>d</sup>Physique de la Matière Condensée, CNRS, Ecole Polytechnique, Institut Polytechnique de Paris, 91128 Palaiseau, France

## Abstract

Silicon nanowire (SiNW) radial junction (RJ) solar cells using hydrogenated microcrystalline silicon ( $\mu\text{-Si:H}$ ) as absorber material have been studied. Since 2013, the performance of such RJ devices has been limited by the low fill factor (FF) and open-circuit voltage ( $V_{OC}$ ). Thanks to the use of n-type hydrogenated microcrystalline silicon oxide ( $\mu\text{-SiO}_x\text{:H}$ ) as a bottom doped layer, we developed the  $\mu\text{-Si:H}$  RJ solar cells with an FF of 69.7% and a  $V_{OC}$  of 0.41 V yielding a power conversion efficiency of 4.1%, which is more than 40% higher than the previously published efficiency record of 2.9%. Our study highlights the role of n-type  $\mu\text{-SiO}_x\text{:H}$  in the improvement of FF.

## 1. Introduction

The use of hydrogenated microcrystalline silicon ( $\mu\text{-Si:H}$ ) as absorber material for photovoltaic (PV) applications has a long history and has led to a multitude of innovative results.<sup>[1–5]</sup> Its incorporation in core-shell silicon nanowires (NWs) was successfully realized in 2012 by Adachi.<sup>[6]</sup> These radial junction (RJ) devices demonstrated a better light-trapping with in particular a higher short-circuit current than thicker  $\mu\text{-Si:H}$  planar devices. A drastic decrease of the reflectance, characterized by in-situ spectroscopy ellipsometry, during the growth of SiNWs was observed.<sup>[7,8]</sup> However, the fill factor (FF) and the open-circuit voltage ( $V_{OC}$ ) of RJ devices were slightly smaller than these measured on the planar reference device<sup>[9]</sup>, leading to an efficiency of 2.9% for these  $\mu\text{-Si:H}$  radial junctions.

In spite of these low efficiency values, it must be kept in mind that the efficiency records of  $\mu\text{-Si:H}$  planar solar cells are in the range of 8.6–11.9%.<sup>[10,11]</sup> Thus there is a strong potential for efficiency increase in  $\mu\text{-Si:H}$  radial junction solar cells, especially if we refer to other absorber thin-film technologies such as hydrogenated amorphous silicon (a-Si:H), which combined with RJs has demonstrated an efficiency of 9.2%<sup>[12]</sup> that is very close to the planar solar cell record of 10.3%<sup>[13]</sup>.

Our approach for optimizing the  $\mu\text{-Si:H}$  p-i-n RJ is to replace p-type and n-type doped  $\mu\text{-Si:H}$  layers by hydrogenated microcrystalline silicon oxide ( $\mu\text{-SiO}_x\text{:H}$ ). Indeed, as a doped layer commonly used in silicon thin film solar cells,  $\mu\text{-SiO}_x\text{:H}$  offers great interest: wider band gap (1.9–2.9 eV)<sup>[14]</sup>, low refractive index ( $\sim 2$ )<sup>[15]</sup> and reasonably high conductivity ( $> 1 \text{ S/cm}$ )<sup>[16]</sup>. Many studies in the past have used  $\mu\text{-SiO}_x\text{:H}$  layers to improve the performance in thin films solar cells. Despeisse *et al.*<sup>[17]</sup> used a n-type doped  $\mu\text{-SiO}_x\text{:H}$  as bottom doped layer in the n-i-p structure silicon solar cells and succeeded to increase the FF by 7.5%. A same finding for Kim *et al.*<sup>[18]</sup>

that improved FF and  $V_{OC}$  by 4.7% and 3%, respectively, using n-type doped  $\mu\text{-SiO}_x\text{:H}$ . In 2015, Misra *et al.*<sup>[12]</sup> used  $\mu\text{-SiO}_x\text{:H}$  as a window layer in a-Si:H RJ solar cells, improving the short-circuit current density by 6.6%.

In this article, we have developed  $\mu\text{-Si:H}$  RJs solar cells by implementing  $\mu\text{-SiO}_x\text{:H}$  as doped layers. For this purpose, the structural, optical and electrical properties of these layers were first studied in a planar configuration and then implemented on RJs SiNWs.

## 2. Experimental details

Sample preparation starts with 1 inch by 1 inch Corning glass (Cg) substrates (type 1737). The back contact structure was either Cg/ZnO:Al or Cg/Ag/ZnO:Al where ZnO:Al refers to aluminum doped zinc oxide (ZnO) with a thickness of 120 nm and Ag refers to silver as a back reflector with a thickness of 160 nm. The layers of Ag and ZnO:Al were deposited via magnetron sputtering. Based on previous research experiences<sup>[12,19,20]</sup>, a very thin layer of Sn with a nominal thickness of  $\sim 1 \text{ nm}$  was deposited on the surface of ZnO:Al via vacuum evaporation ( $< 10^{-6} \text{ mbar}$ ). The metal Sn was used as the catalyst to grow SiNWs. After that, the samples were transferred into a plasma-enhanced chemical vapor deposition (PECVD) reactor dedicated to the growth of doped SiNWs. N-type doped SiNWs were fabricated at  $\sim 410 \text{ }^\circ\text{C}$  in the PECVD reactor with a capacitively coupled radio frequency (RF) discharged at 13.56 MHz, the gas sources of silane ( $\text{SiH}_4$ ), hydrogen ( $\text{H}_2$ ) and phosphine ( $\text{PH}_3$ ) under a pressure of 2.15 mbar and a power density of  $20 \text{ mW/cm}^2$ . The gas flow rates of  $\text{H}_2$ ,  $\text{SiH}_4$  and  $\text{PH}_3$  are 200 sccm, 5 sccm and 0.4 sccm, respectively. As shown in the Supplementary material (S1-Fig. S1), the lengths of SiNWs were calibrated with the duration of growth.

After the growth of n-type SiNWs, the samples were transferred to another PECVD reactor<sup>[21]</sup> optimized for the deposition of thin film layers with the objective of

developing a n-i-p structure. A sequence of layers, namely n-type doped  $\mu\text{-SiO}_x\text{:H}$  (~20 nm) or n-type doped  $\mu\text{-Si:H}$  (~20 nm), intrinsic layer of  $\mu\text{-Si:H}$  (~375 nm), p-type doped  $\mu\text{-SiO}_x\text{:H}$  (~10 nm) and p-type doped  $\mu\text{-Si:H}$  (~10 nm) were deposited on SiNWs at the temperature of 150 °C. P-type and n-type films were respectively obtained by adding trimethylborane (TMB, 1 % diluted in  $\text{H}_2$ ) or phosphine ( $\text{PH}_3$ , 0.1 % diluted in  $\text{H}_2$ ). The oxide layers of n-type (or p-type)  $\mu\text{-SiO}_x\text{:H}$  were made by adding  $\text{CO}_2$  as the O source into the mixture gas of  $\text{SiH}_4$ ,  $\text{H}_2$  and  $\text{PH}_3$  (or TMB) during the PECVD process. All these effective thicknesses were estimated through a previous study that aimed to calibrate the thickness of the thin film shell layer on SiNW core. This calibration process has been performed with respect to reference planar layers deposited on Cg glass substrates (see Supplementary material S2-Fig. S2).

The top layer of the RJ solar cells is made of indium tin oxide (ITO) used as a front transparent electrode with a thickness of ~160 nm. This layer was deposited using magnetron sputtering at the pressure of  $6.3 \times 10^{-3}$  mbar with a RF power of 200 W for 7 min at room temperature under a shadow mask. The contact area of ITO is circular with a diameter of 4 mm.

For this study, we have prepared four samples (n1, n2, n3 and n4), the structure of which from bottom to top is detailed in Table 1. The difference between samples n1 and n2 is that n1 used n-type doped  $\mu\text{-Si:H}$  while n2 used n-type doped  $\mu\text{-SiO}_x\text{:H}$ . For sample n3, we added a silver (Ag) back reflector between Cg and ZnO:Al, and for sample n4, we decreased the length of SiNWs from ~800 nm to ~500 nm.

Before current density-voltage (J-V) and external quantum efficiency (EQE) characterizations, the RJ solar cells were annealed at 200 °C for 15 min. The J-V characterizations were done under the global AM 1.5 sunlight illumination (100 mW/cm<sup>2</sup>). The EQE characterizations were done using a FTSP (Fourier-Transform Photocurrent Spectroscopy) set-up [22] adapted from a FTIR Spectrometer (Thermo Scientific, Nicolet™ iS50 FTIR Spectrometer).

Samples	bottom			top
n1	Cg/ ZnO:Al	SiNWs (n) ~800 nm	$\mu\text{-Si:H(n)}$	$\mu\text{-Si:H(i)}/$
n2			$\mu\text{-SiO}_x\text{:H(p)}/$	
n3	Cg/ Ag/ZnO:Al	SiNWs (n) ~500 nm	$\mu\text{-SiO}_x\text{:H(n)}$	$\mu\text{-Si:H(p+)}/$
n4			ITO	

Table 1: Structure details for samples n1-n4 from bottom to top.

A substantial part of this study was initially conducted on planar layer samples deposited on Cg as references. In this way, we have characterized several groups of planar layers, namely n-type doped  $\mu\text{-SiO}_x\text{:H}$ , intrinsic  $\mu\text{-Si:H}$ , p-type doped  $\mu\text{-SiO}_x\text{:H}$  and p-type doped  $\mu\text{-Si:H}$ . The preparation conditions of these materials are shown in Supplementary material (S3). The crystalline fraction and electrical properties were characterized using Raman spectroscopy (HORIBA, LabRAM HR Evolution), and 4-probes measurements. The illustrations of these characterizations are shown in the Supplementary material (S4-Fig.S3 – Fig.S4).

The morphologies of SiNWs and RJs were characterized

by scanning electron microscopy (SEM, Hitachi S4800 FEG-SEM, acceleration voltage: 10 kV). The density of SiNWs was analyzed by applying ImageJ software [23] to the SEM images.

### 3. Results and discussion

#### 3.1. Electrical and optical properties of reference planar layers on Cg

To estimate the electrical and optical properties of the thin film layers sequentially deposited on SiNWs, we characterized them in the planar configuration, as previously explained. In S4-Fig.S3, from the Raman characterization results, the crystalline fraction of intrinsic and p-type doped  $\mu\text{-Si:H}$ , n-type doped and p-type doped  $\mu\text{-SiO}_x\text{:H}$  were calculated at about 68%, 54%, 45% and 18%, respectively. The conductivity of these layers versus the temperature is illustrated in S4-Fig.S4. The Arrhenius plots highlight an activation energy of  $621 \pm 30$  meV for the intrinsic  $\mu\text{-Si:H}$ , which is close to half the band gap of this material. The activation energies of the p-type  $\mu\text{-Si:H}$ , n-type and p-type  $\mu\text{-SiO}_x\text{:H}$  layers reveal low activation energies of  $19.2 \pm 0.5$  meV,  $79.2 \pm 0.9$  meV and  $94.1 \pm 2.2$  meV, respectively.

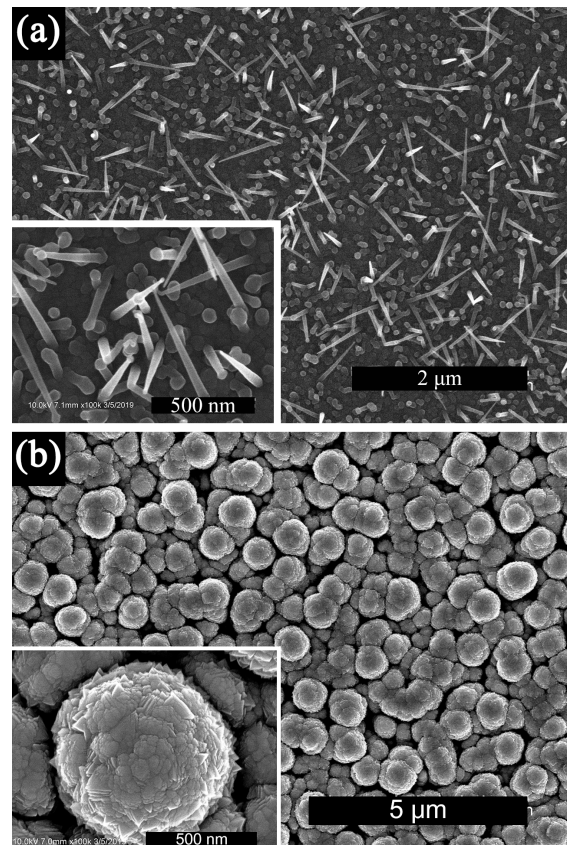


Figure 1: (a) SEM image of SiNWs grown on ZnO:Al surface, the inset shows a high magnification image of SiNWs. The scale bars correspond to 2  $\mu\text{m}$  and 500 nm, respectively. (b) SEM image of complete  $\mu\text{-Si:H}$  RJ with ITO coating, the inset shows a high magnification image of the RJs. The scale bars correspond to 5  $\mu\text{m}$  and 500 nm, respectively.

#### 3.2. Morphology characterization of SiNWs and RJ structure

The evolution of the morphology of the devices, from bare NWs to the finalized RJ structure, was analyzed by SEM. SEM images of n-type SiNWs with a density of  $\sim 6 \times 10^8$

/cm<sup>2</sup>, a diameter of  $\sim 40$  nm and a length of  $\sim 500$  nm are shown in Figure 1(a). After the deposition of n-i-p and ITO layers, SEM images of RJs with a diameter of  $\sim 820$  nm and a density of  $\sim 0.7 \times 10^8$  /cm<sup>2</sup> are shown in Figure 1(b). Regarding the final density, it has been reduced by almost one order of magnitude pointing out nanowire coalescence taking place during the RJ fabrication [24].

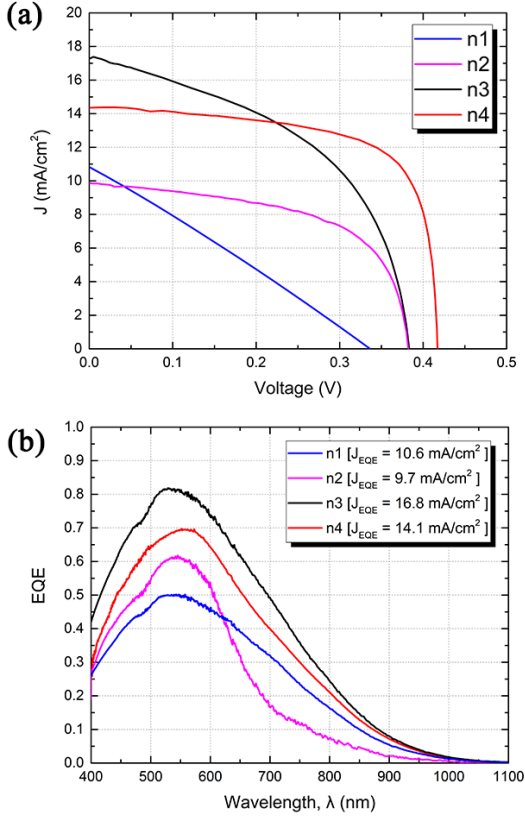


Figure 2: Performance of samples n1-n4 RJ solar cells. (a) J-V characteristics under AM 1.5 global illumination (100 mW/cm<sup>2</sup>). (b) EQE spectra of samples n1-n4 RJ.

### 3.3. Fill Factor improvement

Figure 2 displays the J-V curve and EQE spectra of the RJ solar cell samples (n1-n4). Note that the device surface area is 12.6 mm<sup>2</sup>. The detailed performances of samples n1-n4 are listed in Table 2. Fitted series resistance  $R_s$  and shunt resistance  $R_{sh}$  were determined from the slopes of the J-V curves at  $V=0$  and  $V=V_{OC}$  under illumination in the Figure 2(a) using ‘‘Slope method’’.[25]

Sample	V <sub>oc</sub> V	J <sub>sc</sub> mA/cm <sup>2</sup>	FF %	R <sub>s</sub> Ω cm <sup>2</sup>	R <sub>sh</sub> Ω cm <sup>2</sup>	η %
n1	0.34	10.9	26.6	27.6	9	0.99
n2	0.39	9.8	57.8	2.3	277	2.21
n3	0.38	17.3	49.3	2.3	78.3	3.24
n4	0.41	14.4	69.7	0.7	781	4.13

Table 2: Solar cell parameters of samples n1-n4.

As can be seen from Table 1, sample n1 differs from the others in that the n-doped layer is  $\mu\text{-Si:H}$  instead of  $\mu\text{-SiO}_x\text{:H}$ , and leads to a device with the poorest performances (Table 2).

The low FF value evidenced for n1 seems to be mostly associated with a low shunt resistance value (see Table 2). Replacing the n-type doped  $\mu\text{-Si:H}$  by a wider bandgap

material, i.e. n-type doped  $\mu\text{-SiO}_x\text{:H}$ , greatly improves the FF, in particular by increasing the shunt resistance from  $9 \Omega \text{ cm}^2$  to  $277 \Omega \text{ cm}^2$ .

When comparing samples n2, n3 and n4, all three of which include n-type and p-type  $\mu\text{-SiO}_x\text{:H}$  layers, a large J<sub>SC</sub> difference can be seen between the n2 sample and the others. Indeed, sample n2 is the only one in this series that does not have an Ag back reflector, highlighting its importance even in the context of NW structures that efficiently trap the light.

Samples n3 and n4 are the RJ devices displaying the best performances. A higher J<sub>SC</sub> was obtained for n3 due to the fact that the SiNWs were longer (800 nm compared to 500 nm). However, V<sub>OC</sub> and FF reveal the best improvements when reducing the length to 500 nm (case of sample n4). This suggests issues of non-conformal coverage for longer nanowires, already observed by other studies [26–28], due to coalescence of nanowires and shadowing effects.

The sample n4 with nanowires length of 500 nm shows the highest power conversion efficiency reported so far, with the following solar cell parameters: J<sub>SC</sub> = 14.4 mA/cm<sup>2</sup>, FF = 69.7%, V<sub>OC</sub> = 0.41 V, and η = 4.1%. As illustrated in S4-Fig.S5 in Supplementary material, the devices studied in sample n4 show a homogeneous V<sub>OC</sub> around 0.41-0.42 V, while J<sub>SC</sub> and FF show a variation of less than 10%.

The EQE spectra of samples n1-n4 are shown in Figure 2(b) and match well the expected absorption range of  $\mu\text{-Si:H}$  solar cells.[10,11] The extracted short circuit current density, named J<sub>EQE</sub> is the integrated current density of the EQE spectra in Figure 2(b), which agrees to the J<sub>SC</sub> obtained from J-V measurements with less than 3% difference.

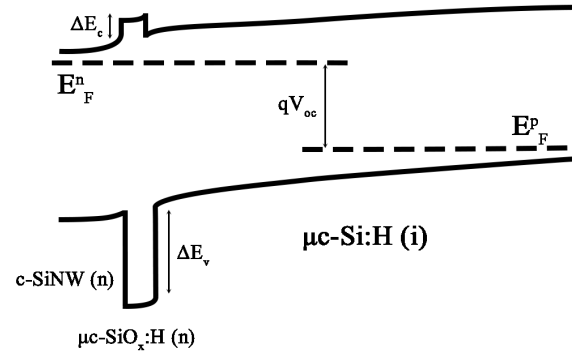


Figure 3: Schematic drawing of band diagram of the n-i (from n-type to intrinsic) junction with the n-type  $\mu\text{-SiO}_x\text{:H}$  as the bottom doped layer under the illumination.

Compared to the results of Adachi *et al.*[9], the most significant improvement of our RJ devices concerns the FF, which is almost 40% higher thanks to the use of  $\mu\text{-SiO}_x\text{:H}$  doped layers instead of  $\mu\text{-Si:H}$  ones. Note that the distribution and the orientation of SiNWs are random, as shown in Figure 1(a), implying that electrical interconnections may form during the fabrication of the RJ [12,19,20,27] and results in the degradation of the shunt resistance. The use of  $\mu\text{-SiO}_x\text{:H}$  seems more favorable to minimize the effects of interconnection, and has in particular improved the V<sub>OC</sub>. The latter point has also been studied and reported for other types of thin film solar cells.[16,17,29] In order to understand the higher V<sub>OC</sub> and shunt resistance of the cells incorporating a n-type  $\mu\text{-SiO}_x\text{:H}$  layer, let us consider the energy band gap diagram

of the n-i-p junction, as schematically illustrated in Figure 3. The introduction of the  $\mu\text{-SiO}_x\text{:H}$  layer leads to the presence of a significant valence band offset barrier that repels the holes generated in the intrinsic  $\mu\text{-Si:H}$  layer reducing the recombination at the interface with the c-SiNW (n) core, therefore improving both FF and  $V_{OC}$ .

#### 4. Conclusions

In this study, we have fabricated SiNW RJ solar cells with  $\mu\text{-Si:H}$  as absorber material. We have developed and implemented  $\mu\text{-SiO}_x\text{:H}$  doped layers to replace standard  $\mu\text{-Si:H}$ . This approach has been particularly efficient to increase the shunt resistance and the  $V_{OC}$ . Ag back reflector has demonstrated to be necessary to strongly increase  $J_{SC}$  values. Finally, reducing the length of the nanowires resulted in a solar cell efficiency of 4.1%, which is the best efficiency reported so far for the  $\mu\text{-Si:H}$  RJ technology. These results show that there is a strong potential for improvement, in particular by focusing on adjusting density and length of SiNWs for an optimized conformal coverage.

#### Abbreviations

SiNW: silicon nanowire; RJ: radial junction;  $\mu\text{-Si:H}$ : hydrogenated microcrystalline silicon; FF: fill factor;  $V_{OC}$ : open-circuit voltage;  $J_{SC}$ : short-circuit current density;  $\mu\text{-SiO}_x\text{:H}$ : hydrogenated microcrystalline silicon oxide; PV: photovoltaic; NWs: nanowires; a-Si:H: amorphous silicon; ZnO: zinc oxide; Al: aluminum; Ag: silver; Cg: corning glass; PECVD: plasma-enhanced chemical vapor deposition; RF: radio frequency;  $\text{SiH}_4$ : silane;  $\text{H}_2$ : hydrogen;  $\text{PH}_3$ : phosphine; ITO: indium tin oxide; J-V: circuit density-voltage; EQE: external quantum efficiency; AM: air mass; FTPS: Fourier-Transform Photocurrent Spectroscopy; FTIR: Fourier Transform InfraRed; SEM: scanning electron microscopy;  $J_{EQE}$ : integrated current density of the EQE spectra; c-SiNW: crystalline silicon nanowire.

#### Supplementing Information

Supporting Information is available from the Wiley Online Library or from the author.

#### Funding

This work was financially supported by the project "SOLARIUM" ANR14-CE05-0025 of the French Research National Agency – project SOLARIUM (ANR).

#### Acknowledgements

The authors are grateful for the funding support received from the French Research National Agency (ANR) of "SOLARIUM" project (ANR14-CE05-0025). The authors especially would like to thank C. Longeaud (GeePs-IPVF) for the access to the EQE measurement equipment.

#### Conflict of Interest

The authors declare no conflict of interest.

#### Keywords

silicon nanowires; radial junction solar cells; plasma-enhanced chemical vapor deposition; hydrogenated microcrystalline silicon oxide ( $\mu\text{-SiO}_x\text{:H}$ ); hydrogenated microcrystalline silicon ( $\mu\text{-Si:H}$ ).

#### References:

- [1] S. Usui, M. Kikuchi, *J. Non. Cryst. Solids* **1979**, *34*, 1.
- [2] J. Meier, R. Flückiger, H. Keppner, A. Shah, *Appl. Phys. Lett.* **1994**, *65*, 860.
- [3] A. Matsuda, in *J. Non. Cryst. Solids*, North-Holland, **2004**, pp. 1–12.
- [4] P. Roca i Cabarrocas, A. Fontcuberta i Morral, B. Kalache, S. Kasout, in *Solid State Phenom.*, Trans Tech Publications Ltd,

- [5] B. Rech, T. Repmann, M. N. van den Donker, M. Berginski, T. Kilper, J. Hüpkes, S. Calnan, H. Stiebig, S. Wieder, *Thin Solid Films* **2006**, *511–512*, 548.
- [6] M. M. Adachi, *Development and Characterization of PECVD Grown Silicon Nanowires for Thin Film Photovoltaics*, **2012**.
- [7] L. Yu, B. O'Donnell, P. J. Alet, P. Roca i Cabarrocas, *Sol. Energy Mater. Sol. Cells* **2010**, *94*, 1855.
- [8] Z. Mrazkova, M. Foldyna, S. Misra, M. Al-Ghazaiwat, K. Postava, J. Pištora, P. Roca i Cabarrocas, *Appl. Surf. Sci.* **2017**, *421*, 667.
- [9] M. M. Adachi, M. P. Anantram, K. S. Karim, *Sci. Rep.* **2013**, *3*, 1.
- [10] K. Ishizaki, M. De Zoysa, Y. Tanaka, T. Umeda, Y. Kawamoto, S. Noda, *Opt. Express* **2015**, *23*, A1040.
- [11] H. Sai, T. Matsui, H. Kumagai, K. Matsubara, *Appl. Phys. Express* **2018**, *11*, 022301.
- [12] S. Misra, L. Yu, M. Foldyna, P. Roca i Cabarrocas, *IEEE J. Photovoltaics* **2015**, *5*, 40.
- [13] A. Lambertz, F. Finger, R. E. I. Schropp, U. Rau, V. Smirnov, *Prog. Photovoltaics Res. Appl.* **2015**, *23*, 939.
- [14] V. Smirnov, A. Lambertz, S. Tillmanns, F. Finger, *Can. J. Phys.* **2014**, *92*, 932.
- [15] S. J. Jung, B. J. Kim, M. Shin, *Sol. Energy Mater. Sol. Cells* **2014**, *121*, 1.
- [16] A. Lambertz, F. Finger, B. Holländer, J. K. Rath, R. E. I. Schropp, in *J. Non. Cryst. Solids*, North-Holland, **2012**, pp. 1962–1965.
- [17] M. Despeisse, G. Bugnon, A. Feltrin, M. Stueckelberger, P. Cuony, F. Meillaud, A. Billet, C. Ballif, *Appl. Phys. Lett.* **2010**, *96*, 073507.
- [18] S. Kim, H. Lee, J. W. Chung, S. W. Ahn, H. M. Lee, *Curr. Appl. Phys.* **2013**, *13*, 743.
- [19] L. Yu, P.-J. Alet, G. Picardi, I. Maurin, P. R. i Cabarrocas, *Nanotechnology* **2008**, *19*, 485605.
- [20] S. Misra, L. Yu, M. Foldyna, P. Roca i Cabarrocas, *Sol. Energy Mater. Sol. Cells* **2013**, *118*, 90.
- [21] P. Roca i Cabarrocas, J. B. Chévrier, J. Huc, A. Lloret, J. Y. Parey, J. P. M. Schmitt, *J. Vac. Sci. Technol. A Vacuum, Surfaces, Film.* **1991**, *9*, 2331.
- [22] N. Puspitosari, C. Longeaud, R. Lachaume, L. Zeyu, R. Rusli, P. R. i Cabarrocas, in *Phys. Status Solidi Curr. Top. Solid State Phys.*, Wiley-VCH Verlag, **2017**, p. 1700165.
- [23] RASBAND, W. S., <http://imagej.nih.gov/ij/> **2011**.
- [24] J. Tang, J.-L. Maurice, W. Chen, S. Misra, M. Foldyna, E. V. Johnson, P. Roca i Cabarrocas, *Nanoscale Res. Lett.* **2016**, *11*, 455.
- [25] C. Chibbaro, M. Zimbone, G. Litrico, P. Baeri, M. L. Lo Trovato, F. Aleo, *J. Appl. Phys.* **2011**, *110*, 044505.
- [26] L. Yu, B. O'Donnell, M. Foldyna, P. Roca i Cabarrocas, *Nanotechnology* **2012**, *23*, 194011.
- [27] M. Müller, M. Ledinský, J. Kočka, A. Fejfar, J. Červenka, *J. Vac. Sci. Technol. B, Nanotechnol. Microelectron. Mater. Process. Meas. Phenom.* **2018**, *36*, 011401.
- [28] M. Macias-Montero, A. N. Filippin, Z. Saghi, F. J. Aparicio, A. Barranco, J. P. Espinos, F. Frutos, A. R. Gonzalez-Elipe, A. Borrás, *Adv. Funct. Mater.* **2013**, *23*, 5981.
- [29] M. Python, E. Vallat-Sauvain, J. Bailat, D. Dominé, L. Fesquet, A. Shah, C. Ballif, *J. Non. Cryst. Solids* **2008**, *354*, 2258.